Resonance Raman Observation of the Structural Dynamics of FixL on Signal Transduction and Ligand Discrimination†

Yusuke Hiruma,‡ Akihiro Kikuchi,§ Atsunari Tanaka,§,||,⊥ Yoshitsugu Shiro,§ and Yasuhisa Mizutani*,‡,@,#

Graduate School of Science and Technology, Kobe University, Nada, Kobe 657-8501, Japan, Molecular Photoscience Research Center, Kobe University, Nada, Kobe 657-8501, Japan, RIKEN SPring-8 Center, Harima Institute, 1-1-1 Kouto, Sayo, Hyogo 679-5148, Japan, and Yokohama City University International Graduate School of Arts and Sciences, Suehiro, Tsurumi, Yokohama, Kanagawa 230-0045, Japan

Received October 6, 2006; Revised Manuscript Received January 25, 2007

ABSTRACT: FixL is a heme-based O_2 sensor protein, which responds to low O_2 concentrations by activating the transcriptional activator FixJ. Signal transduction is initiated by the dissociation of O_2 from the sensor domain of FixL, resulting in protein conformational changes that are transmitted to a histidine kinase domain. To gain insight into the FixL sensing mechanism, we monitored changes in the protein's structure in the picosecond to millisecond time frame, following the dissociation of the ligand using time-resolved resonance Raman spectroscopy. This study presents the time-resolved resonance Raman spectra of *Sinorhizobium meliloti* FixL upon O_2 dissociation, as well as upon CO dissociation. The FixL spectra show that there are three steps in the dynamic structural changes that result from ligand dissociation. Ligand-dependent structural dynamics are observed in the earliest step. On the basis of comparisons of these structural changes, a scheme for the signal transduction of FixL is proposed which supports the FG loop switch mechanism. Similar spectral changes were observed both for the sensor domain and for the full-length protein, although structural changes occurred faster with the former than with the latter. This difference in rate suggests that the structural changes occurring in the heme pocket are coupled to those of the kinase domain. The implications of these results for FixL's sensing mechanism are discussed.

Heme-based sensors are a class of enzymes which regulate enzymatic activities and DNA binding in response to the presence of the diatomic gas molecules CO, NO, and O_2. The FixL protein found in *rhizobia* senses O_2 and regulates the expression of genes associated with nitrogen fixation as a function of O_2 pressure (*1*−*3*). FixL belongs to the large family of bacterial two-component sensors (*4*), modular proteins typically comprised of a sensor domain and an enzymatic signaling or effector domain. The FixL protein is composed of an ATP-dependent histidine kinase domain at the C-terminus and a heme-based O_2 sensor domain at the N-terminus. The N-terminal domain is a prototypical PAS domain, a ubiquitous protein sensory module found in all kingdoms (*5*), has a conserved α/β fold, and consists of ∼150 residues (*6*).

In the absence of O_2, FixL is autophosphorylated at an invariant histidine residue and the phosphoryl group is transferred to FixJ, leading to enhanced transcriptional activity. Under aerobic conditions, binding of O_2 to the sensor domain suppresses histidine kinase activity in the C-terminal domain by up to 15-fold (*7*). It is believed that structural changes in the vicinity of the heme, caused by the transition between the deoxy and oxy states, constitute the initial event in O_2 sensing. This is followed by intramolecular signal transduction from the heme to the histidine kinase site, thus regulating kinase activity. In the in vitro autophosphorylation assay, however, FixL exhibits broad ligand specificity: CO induces a conformational change, resulting in a 5-fold decrease in FixL kinase activity, while NO and CN^- cause 2- and 15-fold decreases, respectively (*7*).

Recently, several hypotheses for the mechanism of activation, including O_2 selectivity, have been proposed. Crystal structures of the sensor domains of FixL (*6*, *8*−*11*) have provided some notable findings on differences between the liganded and unliganded forms. Structures of the sensor domain bound to CN^- and O_2 show that ligand binding results in a structural change in the FG loop of the protein, termed the FG loop switch (*6*, *9*, *10*). This change is accompanied by a reorientation of the Arg214 side chain

† This work was supported by a Grant-in-Aid for Scientific Research (B) (Grant 17350009) from the Japan Society for the Promotion of Science to Y.M., a Grant-in-Aid for Specially Promoted Research (Grant 14001004) from the Ministry of Education, Culture, Sports, Science and Technology of Japan to Y.M., and a Grant-in Aid for Scientific Research on Priority Areas (16074217 "Chemistry of Coordination Space") from the Ministry of Education, Culture, Sports, Science and Technology of Japan to Y.S.

* To whom correspondence should be addressed. E-mail: mizutani@ch.wani.osaka-u.ac.jp. Phone: +81-6-6850-5776. Fax: +81-6-6850-5785.

‡ Graduate School of Science and Technology, Kobe University.

§ RIKEN SPring-8 Center.

|| Yokohama City University International Graduate School of Arts and Sciences.

⊥ Current address: Institute of Multidisciplinary Research for Advanced Materials, Tohoku University, 2-1-1 Katahira, Aoba-ku, Sendai 980-8577, Japan.

@ Molecular Photoscience Research Center, Kobe University.

Current address, Graduate School of Science, Osaka University, 1-16 Machikaneyama, Toyonaka 560-0043, Japan.

10.1021/bi062083n CCC: $37.00
Published on Web 05/01/2007

(corresponding to Arg220 in *Bj*FixL)[1] in the heme pocket and the formation of a hydrogen bond with the bound ligand. In contrast, despite the fact that the CO-bound form adopts a low-spin complex comparable to the CN^- and O_2 complexes, its structure was reported to be nearly identical to that of *Bj*FixL bound to high-spin heme in the met and deoxy form (*6*, *10*). On the basis of these findings, Hao et al. (*10*) proposed a regulatory mechanism based on structural changes in the FG loop of the protein. Ligand binding converts the domed, high-spin heme in the deoxy state into a planar low-spin hexacoordinate state. These structural changes in the heme plane are accompanied by displacement of the heme propionate groups. Displacement of the carboxylate of heme propionate 7 weakens its salt bridge to the side chain of Arg214, prompting replacement of this group at the propionate with the side chain of Arg200 (corresponding to Arg206 in *Bj*FixL). Arg214 then moves into the binding pocket where it forms a hydrogen bond with the bound oxygen, creating a steric clash with Ile209 (corresponding to Ile215 in *Bj*FixL) and producing a 2 Å shift in the FG loop. The greater sensitivity of FixL to O_2 and CN^- than to other ligands can be explained by this model, since O_2 and CN^- are capable of holding the released Arg214 in the heme pocket. Nonetheless, other factors must be involved in the inhibition of phosphorylation activity in CO-, NO-, and imidazole-bound forms of FixL, because in those structures, movement of Arg214 into the pocket is not observed (*12*). Dunham and co-workers (*8*) showed that the X-ray structure of the met R220A mutant has a dramatically lowered affinity for O_2, but CO binding remains unchanged. Interestingly, CN-bound R220A mutants retain some ability to weakly inhibit FixL in the absence of the FG loop switch. This finding suggests that Arg214 cannot be the sole factor in kinase regulation (*8*).

Another mechanism proposed for signal recognition is that the conformational change is driven by steric interaction between the bound ligand and distal hydrophobic residues (*13*). The ligand binding pocket of FixL contains three conserved hydrophobic side chains, termed the hydrophobic triad: Ile209, Leu230, and Val232 in *Sm*FixL and Ile215, Leu236, and Ile238 in *Bj*FixL. Each of these side chains must be displaced to bind the ligand, with this displacement giving rise to a signal in the form of structural changes within the protein.

To understand the FixL O_2-sensing mechanism, it is necessary to understand changes in the structure of the heme and the heme environment induced by O_2 association and dissociation. Although X-ray crystallographic studies provide information about the two end point structures (liganded and unliganded FixL), no information about how the structural changes propagate from the heme to the kinase domain is provided. To elucidate this mechanism, time-resolved structural data on the FixL intermediates are required. To date, such structural dynamics information, providing a molecular basis for understanding the mechanism of intramolecular signal transduction from the heme to the kinase domain in FixL, has not been available. Furthermore, no X-ray crystallographic data are available for the protein with the kinase domain; the proposed models are based on crystallographic data of the sensor domain. It is unclear whether the model proposed on the basis of these sensor domain data is valid for the intact FixL protein.

In this study, time-resolved resonance Raman (RR) was used to follow dissociation of the ligand from FixL. RR spectroscopy is a powerful tool for studying both the structure of the heme and its binding pocket in heme proteins; therefore, time-resolved RR spectroscopy enabled us to observe the structural changes occurring in the functioning protein (*14*, *15*). No time-resolved vibrational studies of FixL aimed at elucidating the structural dynamics of the protein following ligand dissociation have been previously reported, although single-color resonance Raman experiments were conducted by Rodgers et al. (*16*). We compared the time-resolved RR data for the O_2- and CO-dissociated forms to determine the protein dynamics important for ligand discrimination. The observed dynamics are discussed in the context of differences between the O_2- and CO-dissociated forms. We also compare the results obtained for the sensor domain (*Sm*FixLH2) with soluble FixL containing the sensor domain and the kinase domain (*Sm*FixL). The rates at which spectral changes occurred were found to be different, suggesting that the observed structural changes are coupled to changes in the kinase domain. These results strongly suggest that the rearrangement of Arg214 is a key step in signal transduction and ligand discrimination in FixL.

EXPERIMENTAL PROCEDURES

Sample Purification. The *Sm*FixL used in this study, in which Cys301 was mutated to Ala to prevent aberrant dimer formation, was expressed in *Escherichia coli* and purified using a modification of the method described previously (*17*). In brief, the protein was purified to homogeniety from *E. coli* extract using a TARON His tag affinity column (CLONTECH), followed by ion exchange UNO Q (Bio-Rad) chromatography with a linear gradient elution from 0 to 1.0 M NaCl in 20 mM Tris-HCl (pH 9) containing 5% glycerol. The *Sm*FixL fraction was dialyzed against 20 mM Tris-H_2SO_4 buffer (pH 8) containing 5% glycerol. The *Sm*FixLH2 was expressed and purified as described previously (*17*), but the His tag step was eliminated. Thus, both the *Sm*FixL and *Sm*FixLH2 proteins used in this study are six-His-tagged at the N-terminus.

Sample Preparation. The protein concentration for the time-resolved RR measurements was 80 μM in 20 mM Tris-H_2SO_4 (pH 8.0) containing 5% (v/v) glycerol. Deoxy and CO-bound forms of FixL were prepared by filling the sample cell containing the met form with 100% N_2 and CO gas, respectively, and then adding a solution of sodium dithionite (final concentration of 1 mM). The oxy form was prepared by adding DTT (final concentration of 10 mM) to the sample cell containing the met form under a 100% O_2 atmosphere.

Raman Measurements. Picosecond time-resolved RR measurements were performed as described previously (*15*). Pump pulses at 540 nm (15 μJ/pulse, 1 kHz) were generated by a home-built OPG/OPA device pumped by the second harmonic of the output of a Ti:sapphire regenerative amplifier

[1] Abbreviations: *Sm*FixL, soluble truncated form of *Sinorhizobium meliloti* FixL containing both heme and kinase domains; *Sm*FixLH2, *Sm*FixL sensor domain; *Bj*FixL, *Bradyrhizobium japonicum* FixL; DTT, dithiothreitol; RR, resonance Raman; CO-FixL, ferrous FixL bound to carbon monoxide; met-FixL, unligated ferric FixL; oxy-FixL, ferrous FixL bound to oxygen; deoxy-FixL, unligated ferrous FixL; WT, wild type.

(Spitfire, Positive Light) seeded by a picosecond Ti:sapphire oscillator (Tsunami, Spectra Physics). Probe pulses at 442 nm (0.3 μJ/pulse) were generated by stimulated Raman scattering in compressed methane gas excited by the second harmonic. Nanosecond time-resolved RR measurements were performed with two nanosecond pulse lasers operating at 10 Hz. Probe pulses at 436 nm were generated by focusing the 532 nm second harmonic from an Nd:YAG laser (Surelight II, Continuum) into a hydrogen-shifting cell operated at 0.9 MPa. The Raman-shifted lines were separated using a Pellin-Broca prism, and the desired 436 nm line was line-focused onto a spot on the sample. The probe power was as low as possible (50 and 300 μJ/pulse for the CO- and O_2-bound forms, respectively) to prevent the ligand photodissociation by the probe pulse. The amount of photodissociation induced by the probe beam itself was estimated to be as little as 4%. The pump beam 532 nm output was the second harmonic of an Nd:YAG laser (Minilight II, Continuum), and its power was adjusted to 0.7 and 7 mJ/pulse for the CO and O_2 dissociation, respectively. These pump and probe beams were directed collinearly using a dichroic mirror and focused onto the sample cell with spherical and cylindrical lenses. The timing between pump and probe pulses was adjusted with a computer-controlled pulse generator (DG 535, Stanford Research Systems) via a GPIB interface. Time-resolved RR data acquisition was carried out as described previously (*15*). The time delay of the probe pulse with respect to the pump pulse was determined by detecting the two pulses with a photodiode (ET-2000, Electro-Optics Technology) just before the sample point and monitoring with an oscilloscope (DS-4262, Iwatsu). Jitters in the delay time were within $\pm$2 ns. CW RR spectra of FixL were measured using the 410 nm line of a frequency-doubled diode laser provided by Matsushita Electric Industrial Co., Ltd.

The sample solution was contained in a 10 mm NMR tube and spun with a spinning cell device designed to minimize off-center deviation during rotation. Raman scattered light was collected at 135° with a pair of fused quartz lenses, f-matched to a 0.65 m spectrograph (Triplemate1877, Spex) which was equipped with a holographic grating (2400 grooves/mm) and a liquid nitrogen-cooled CCD detector (LN/CCD 1100PB, Princeton Instruments). A depolarizer was used to scramble the polarization of the collected light and thus eliminate intensity artifacts created by polarization-dependent grating reflectivity. The spectra were calibrated using the standard Raman spectra of cyclohexane and carbon tetrachloride.

RESULTS

CO Dissociation. Figure 1 shows nanosecond time-resolved RR spectra of CO-*Sm*FixL upon ligand photodissociation for various delay times of the probe pulse with respect to the pump pulse. In these spectra, the contribution of unphotolyzed species has been subtracted. Spectral intensities can vary due to structural changes in the photolyzed species and due to population changes in the photolyzed species resulting from ligand recombination. To eliminate the contribution of the population change from the observed intensity change, the Raman intensity at each delay time has been normalized using the band intensity of the ν_7 mode (breathing-like mode of the porphyrin inner ring). Justification for using the ν_7 band as an internal standard

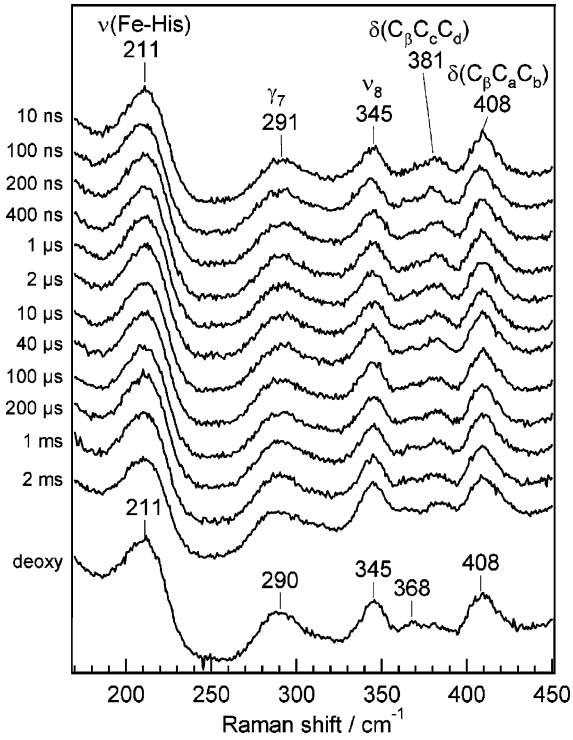

FIGURE 1: Nanosecond time-resolved RR spectra at the indicated delay times following the photolysis of CO-*Sm*FixL. The RR spectrum of deoxy-*Sm*FixL is shown at the bottom for comparison.

for comparing the intensities of low-frequency modes has been presented for carbonmonoxy hemoglobin (*18*). Franzen et al. calibrated the intensity of the ν_7 band against the sulfate band from ammonium sulfate for hemoglobin. They found that the ν_7 band can be used as an internal standard. Since FixL and hemoglobin have the common heme (iron protoporphyrin IX complex) and the common axial ligand from the protein (His), it is a reasonable and credible assumption that the ν_7 band can be used as an internal standard for FixL as well. The bands at 221, 291, 345, 380, and 408 cm^{-1} in the 10 ns delay spectrum are assigned to vibrations of the heme. The RR band at 221 cm^{-1} arises from the stretching mode of the covalent bond between the heme iron and the N_ϵ atom of the proximal His, ν(Fe$-$His) (*19*). The band at 291 cm^{-1} is an out-of-plane mode (γ_7; methine wagging) (*20*). The band at 345 cm^{-1} was assigned to ν_8, a metal pyrrole stretch and substituent bend. The bands at 380 and 408 cm^{-1} are substituent modes, $\delta(C_\beta C_c C_d)$, involving deformation of the propionate methylene groups, and δ-$(C_\beta C_a C_b)$, involving deformation of the vinyl groups, respectively. The time-resolved RR spectrum at 10 ns differed from the spectrum of the deoxy form. The relative intensity of the 380 cm^{-1} band with respect to the 368 cm^{-1} band in the 10 ns time-resolved RR spectrum was different from that in the spectrum of the deoxy form. The ν_8 and γ_7 bands in the 10 ns time-resolved RR spectrum were less prominent than those in the spectrum of the deoxy form but became more prominent with an increase in delay time, indicating that the heme structure 10 ns after CO dissociation is different from that of the deoxy structure. To observe this difference more clearly, we calculated the difference spectra between the time-resolved RR spectra and the spectrum of the deoxy form, as shown in Figure 2. Difference features were observed for $\delta(C_\beta C_c C_d)$, ν_8, and γ_7 bands in the 10 ns time

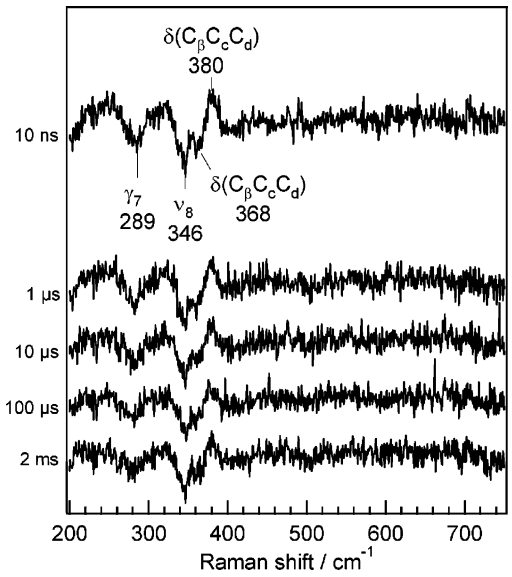

FIGURE 2: Nanosecond time-resolved difference RR spectra at the indicated delay times following the photolysis of CO-*Sm*FixL.

delay spectra. Although the difference features became less pronounced as the delay time increased from 10 ns to 2 ms, they nonetheless remain apparent in the 2 ms spectrum. This indicates that both the structure of the heme and the vicinity of the heme have not fully relaxed to the deoxy structure 2 ms following CO dissociation. No prominent difference was observed in the 200−220 cm^{-1} region, suggesting that the ν(Fe−His) band exhibited neither a frequency shift nor an intensity change in the time window between 10 ns and 2 ms. This suggests that the heme pocket structure of the proximal side does not change significantly following CO dissociation. The vinyl bending $\delta(C_\beta C_a C_b)$ modes were observed as a single band at 408 cm^{-1}; neither the band intensity nor frequency changed following ligand dissociation, indicating that the heme pocket environment around the vinyl groups remains unchanged following ligand dissociation.

The time-resolved RR spectra of CO-*Sm*FixLH2 exhibited features similar to those of CO-*Sm*FixL: intensity decrease of the $\delta(C_\beta C_c C_d)$ band at 380 cm^{-1} and intensity increase of the $\delta(C_\beta C_c C_d)$ band at 369 cm^{-1}, ν_8, and γ_7 bands with delay increases (data shown in Figure S1 of the Supporting Information). The ν(Fe−His) band appeared at 211 cm^{-1} and did not exhibit a frequency shift in the time window between 10 ns and 2 ms.

Figure 3 compares the temporal evolution of the intensity of the ν_8 (A), γ_7 (B), ν(Fe−His) (C), and $\delta(C_\beta C_c C_d)$ (D) bands around 380 cm^{-1} of *Sm*FixL and *Sm*FixLH2 following CO dissociation. The relative intensities of the bands were calculated using the intensity of the deoxy form as a reference. For both *Sm*FixL and *Sm*FixLH2, the ν_8 and γ_7 bands show intensity changes after approximately 100 μs. No appreciable intensity change was observed for the ν(Fe−His) band. For the $\delta(C_\beta C_c C_d)$ band at 380 cm^{-1}, CO-*Sm*FixLH2 exhibited a two-phase intensity change, while CO-*Sm*FixL exhibited a single-phase change in the 10 ns to 1 ms time frame. The slow phase for *Sm*FixL was not observed in this time window. The temporal changes of the $\delta(C_\beta C_c C_d)$ band were fitted using single-exponential and double-exponential functions for *Sm*FixL and *Sm*FixLH2, respectively. The time constants of *Sm*FixLH2 are 0.77 μs and 1.4 ms for the fast and slow phases, respectively, whereas the time constant of *Sm*FixL is 9.1 μs for the fast phase. The time constant of the fast phase of *Sm*FixLH2 was smaller by 1 order magnitude compared to that of *Sm*FixL, suggesting that the kinase domain decelerates the structural dynamics of the heme and heme pocket of the sensor domain. The temporal changes of the ν_8 and γ_7 bands were fitted using a single-exponential function.

To observe fast structural changes in the heme, we measured picosecond time-resolved RR spectra of *Sm*FixLH2 and *Sm*FixL following CO photodissociation. Panels A and B of Figure 4 show picosecond time-resolved RR spectra of *Sm*FixL and *Sm*FixLH2, respectively. Traces a−c represent the time-resolved RR spectra at 20 and 1000 ps delays and a static spectrum of the deoxy form, respectively. Trace d in each panel represents the difference spectrum between traces a and c, while trace e represents the difference spectrum between traces a and b. Trace d demonstrates that the intensity of the $\delta(C_\beta C_c C_d)$ band of the transient species at 20 ps was different from that of the deoxy form, showing that little structural change occurred in the heme between 20 and 1000 ps.

The frequency of the ν(Fe−His) band appears at a position very close to that of the deoxy form in both panels A and B of Figure 4. No frequency change was observed for *Sm*FixL or *Sm*FixLH2 in the picosecond to millisecond region, which is in contrast to the results of Rodgers et al. (*16*). They reported that the photolyzed FixL species measured with a 3 ns probe pulse has the ν(Fe−His) band at 218 cm^{-1}, which is 7 cm^{-1} higher than the frequency of the deoxy form. To address this discrepancy, we measured transient resonance Raman spectra of CO-*Sm*FixLH2 as Rodgers et al. did. Figure 5A shows RR spectra of *Sm*FixLH2 in its deoxy, CO, and photolyzed states. We used the same wavelength (435.8 nm) and pulse energy (300 μJ/pulse) as Rodgers et al., while our pulse width (10 ns) was broader than theirs (3 ns). Trace a contains contributions from the photodissociated and unphotolyzed CO-bound forms. A fresh portion of the CO-*Sm*FixLH2 sample solution was excited with the probe pulse as the sample was spun during the Raman measurements; therefore, trace a does not contain contributions from deoxy-*Sm*FixLH2. Trace b shows a RR spectrum of deoxy-*Sm*FixLH2. Trace c is a difference spectrum obtained by subtracting trace b from trace a. A RR band was observed at 218 cm^{-1} in trace c, which is consistent with Rodgers et al. (*16*). Since trace b is subtracted from trace a to yield trace c, the positive bands in trace c are due to the photodissociated or CO-bound forms. There seem to be positive and negative intensity to the high- and low-frequency side of the ν(Fe−His) band position in Figure 2. This is consistent with a spectral feature reported by Rodgers et al. (*16*). This suggests that the weak band at 218 cm^{-1} can be due to the photodissociated form, although it is not the ν-(Fe−His) band.

There is a possibility that the band at 218 cm^{-1} is due to the CO-bound form. We measured RR spectra while changing the energy of the laser pulse. As seen in Figure 5B, a weaker probe pulse energy results in a higher-frequency band. Because the contribution of the CO-bound form in the spectra increases as the energy of the probe pulse becomes weaker, the observed positive band at 218 cm^{-1} can be

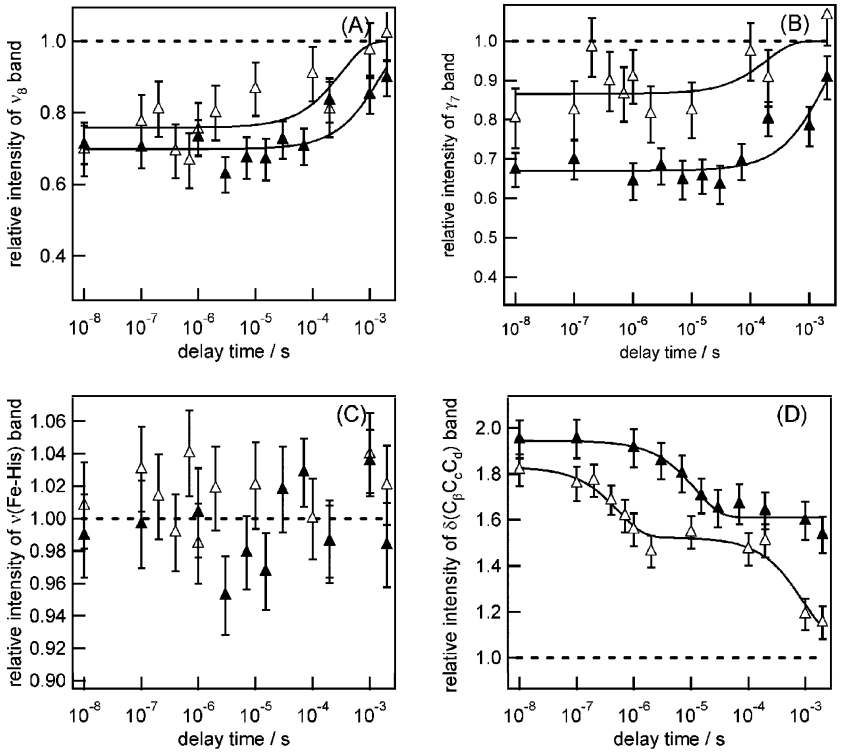

FIGURE 3: Logarithmic time plots of relative intensities for the γ_7, ν_8, ν(Fe−His), and $\delta(C_\beta C_c C_d)$ bands extracted from time-resolved data of CO dissociation. The filled and empty triangles represent the relative intensities of *Sm*FixL and *Sm*FixLH2, respectively. The solid lines indicate the best fit obtained using an exponential decay or a sum of two exponential decays.

ascribed to the CO-bound form. In fact, trace c in Figure 5A is similar to a CW spectrum of CO-*Sm*FixLH2 with 442 nm excitation reported by Rodgers et al. (*16*), where a weak band around 218 cm^{-1} was observed. Trace d in Figure 5A is a RR spectrum of CO-*Sm*FixLH2 measured using a CW laser (410 nm). The laser power was sufficiently low (0.5 mW) that the spectrum contains no contribution from photodissociated species. A weak band at 217 cm^{-1} was observed in trace d, which contains only the contribution from the CO-bound form. Thus, the band around 218 cm^{-1} can be due to either the photodissociated form or the CO-bound form. In either case, the 218 cm^{-1} band in trace c in Figure 5A cannot be assigned to the ν(Fe−His) band of the photodissociated form. Accordingly, these time-resolved data demonstrate that the ν(Fe−His) band shows no frequency shift in the picosecond to millisecond time region.

O_2 Dissociation. Figure 6 shows nanosecond time-resolved RR spectra of oxy-*Sm*FixL upon ligand photodissociation. To eliminate the contribution of population change from the observed intensity change, the Raman intensity at each delay time has been normalized using the ν_7 intensity. The signal-to-noise ratio of the spectrum at 1 ms is low because the amount of photodissociated species is small due to fast recombination of O_2. It should be noted that the intensities of the ν_8 and γ_7 bands 15 ns following O_2 dissociation are lower than that at 10 ns following CO dissociation. As the time delay increased from 15 ns to 1 ms, the intensity of the $\delta(C_\beta C_c C_d)$ band at 380 cm^{-1} decreased and the intensities of the ν_8 band at 345 cm^{-1}, γ_7 band at 291 cm^{-1}, and ν-(Fe−His) band at 211 cm^{-1} increased. *Sm*FixLH2 exhibited time-resolved RR features common to *Sm*FixL upon O_2 dissociation (data shown in Figure S2 of the Supporting Information). As the time delay increased from 15 ns to 1 ms, the intensity of the $\delta(C_\beta C_c C_d)$ band at 381 cm^{-1} decreased and the intensities of the ν_8 band at 345 cm^{-1}, γ_7 band at 292 cm^{-1}, and ν(Fe−His) band increased. These features are common between *Sm*FixL and *Sm*FixLH2.

The temporal behavior of band intensity following O_2 dissociation was compared between *Sm*FixL and *Sm*FixLH2. Figure 7 shows the temporal evolution of the intensity of the ν_8 band (A), γ_7 band (B), ν(Fe−His) band (C), and δ-$(C_\beta C_c C_d)$ band at 380 cm^{-1} (D). These band intensities reflect the relative intensities of the corresponding bands of the deoxy form. The solid lines in each panel represent the curves fit with exponential functions to the observed intensity changes of the Raman bands. The fitting parameters are summarized in Table 1. The temporal evolution of the ν_8 and γ_7 bands of *Sm*FixLH2 exhibited biphasic changes, and their band intensities in the time-resolved RR spectra changed to that of the deoxy form at 1 ms. The fast and slow phases were observed in the submicrosecond and millisecond time frame, respectively. In contrast, the ν_8 and γ_7 bands of *Sm*FixL exhibited single-phase changes in the time window from 15 ns to 1 ms; they exhibited intensity changes in the microsecond time frame, indicating that a phase in the intensity change occurs after 1 ms in *Sm*FixL. Panel C of Figure 7 shows that the ν(Fe−His) bands of *Sm*FixLH2 and *Sm*FixL exhibited only the fast phase. In contrast to the CO-dissociated form (Figure 3C), the temporal change of the band intensity was observed in the 100 ns to 1 μs time range for the O_2-dissociated form. For both *Sm*FixL and *Sm*FixLH2, the time constants of the intensity change for the ν(Fe−His) band were close to those of the fast phase for the ν_8 and γ_7 bands. In panel D, the temporal evolution of the $\delta(C_\beta C_c C_d)$ band of *Sm*FixLH2 showed biphasic changes to unity, with the fast and slow phases observed on the microsecond and millisecond time frame, respectively. The $\delta(C_\beta C_c C_d)$ band of *Sm*FixL showed intensity changes on the microsecond

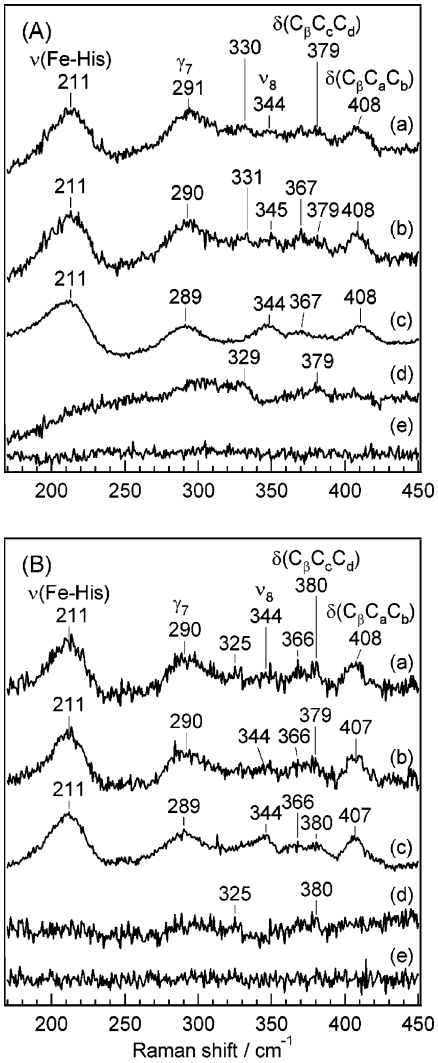

FIGURE 4: Picosecond time-resolved RR spectra following the photolysis of CO-*Sm*FixL (A) and CO-FixLH (B): (a) time-resolved RR spectra with a 20 ps delay, (b) time-resolved RR spectra with a 1000 ps delay, (c) static spectra of deoxy-*Sm*FixL, (d) difference spectra (trace c subtracted from trace a), and (e) difference spectra (trace b subtracted from trace a).

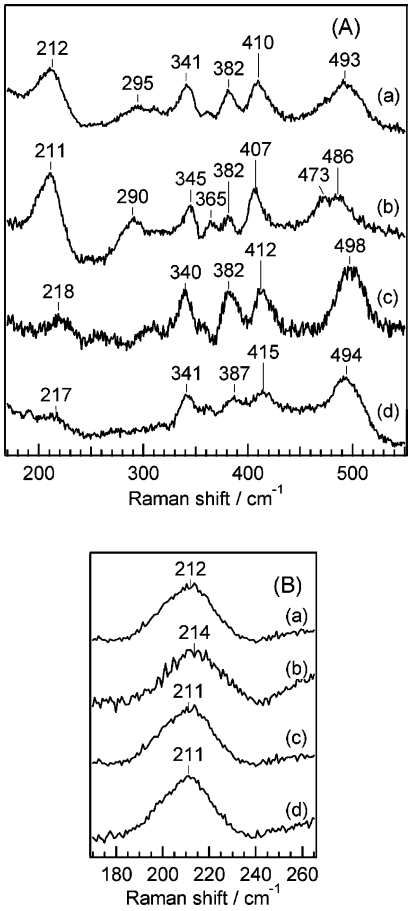

FIGURE 5: (A) RR spectra of deoxy-*Sm*FixLH2, CO-*Sm*FixLH2, and its photoproducts. (a) Partially photolyzed CO-*Sm*FixLH2, 436 nm pulsed excitation, pulse repetition rate of 10 Hz, pulse energy of 300 μJ/pulse. (b) Authentic deoxy-*Sm*FixLH2 recorded with 436 nm pulsed excitation, a pulse repetition rate of 10 Hz, and a pulse energy of 300 μJ/pulse. (c) Difference spectrum obtained by subtraction of trace b from trace a. In obtaining trace c, we used the 211 cm^{-1} band of deoxy-*Sm*FixLH2 as an indicator of when the equilibrium contributions of deoxy-*Sm*FixLH2 had been removed. (d) CO-*Sm*FixLH2 spectrum recorded with 0.5 mW of CW 410 nm excitation. (B) Single-pulse transient RR spectra of partially photolyzed CO-*Sm*FixLH2 measured at different laser pulse energies. (a) CO-*Sm*FixLH2 with 436 nm pulsed excitation, a pulse repetition rate of 10 Hz, and a pulse energy of 300 μJ/pulse. (b) CO-*Sm*FixLH2 with 436 nm pulsed excitation, a pulse repetition rate of 10 Hz, and a pulse energy of 30 μJ/pulse. (c) Difference spectrum obtained by subtraction of trace b from trace a. (d) Authentic deoxy-*Sm*FixLH2 recorded with 436 nm pulsed excitation, a pulse repetition rate of 10 Hz, and a pulse energy of 300 μJ/pulse.

time scale, and band intensities at 1 ms were different from those of the deoxy form, indicating that the intensity changes have a phase later than 1 ms. For both *Sm*FixLH2 and *Sm*FixL, rates in the fast phase of the $\delta(C_\beta C_c C_d)$ band intensity were approximately 3 times lower than those of the other Raman bands. This indicates that the structural change causing the fast phase of intensity changes of the ν_8, γ_7, and ν(Fe−His) bands is not associated with the $\delta(C_\beta C_c C_d)$ band. On the other hand, the rate in the slow phase of the $\delta(C_\beta C_c C_d)$ band intensity of *Sm*FixL was close to that of the other two Raman bands, suggesting that common structural changes give rise to the intensity changes of all three Raman bands. It should be noted that the time evolution of the band intensities of *Sm*FixL was slower than those of *Sm*FixLH2 in terms of the fast and slow phases for the four bands, suggesting that the kinase domain affects the structural dynamics of the heme and the heme environment in the sensor domain.

Comparison between the CO- and O_2-Dissociated Forms of SmFixL. Figure 8 compares the temporal behavior of the intensities of the $\delta(C_\beta C_c C_d)$, ν_8, γ_7, and ν(Fe−His) bands between the CO- and O_2-dissociated forms of *Sm*FixL. In the window between 10 ns and 10 μs, fast intensity changes were observed for the ν_8 and γ_7 bands specific to the O_2-dissociated form. In contrast, there is close similarity in the temporal changes between the CO- and O_2-dissociated forms in the 10 μs to 1 ms time range in panels A and B. The ν(Fe−His) band shows the intensity change for the O_2-dissociated species but not for the CO-dissociated species. The intensity change of the $\delta(C_\beta C_c C_d)$ band was faster for the O_2-dissociated species than for the CO-dissociated species.

DISCUSSION

The temporal evolution of RR bands in time-resolved RR spectra of *Sm*FixL and *Sm*FixLH2 following ligand dissocia-

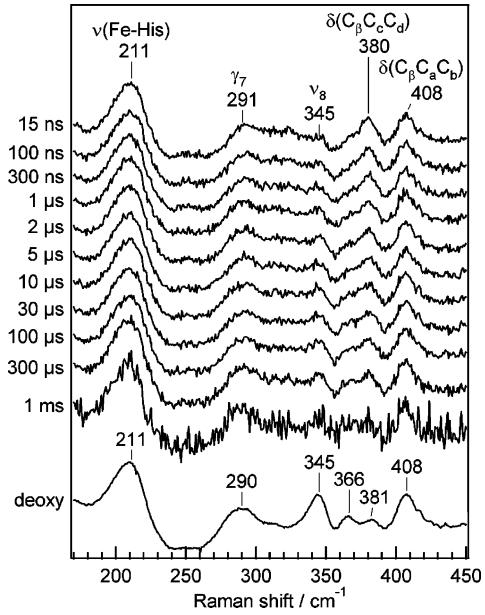

FIGURE 6: Nanosecond time-resolved RR spectra at the indicated delay times following photolysis of oxy-SmFixL. The RR spectrum of deoxy-*Sm*FixL is shown at the bottom for comparison.

tion has been observed for the first time. Spectral changes were observed in both the O_2-dissociated and CO-dissociated species. These spectral changes indicate structural changes in the heme and in the vicinity of the heme in FixL upon ligand dissociation. Changes in the time-resolved RR spectra occurred in three steps. The band intensities of the ν(Fe-His), γ_7, and ν_8 modes changed in 0.2−2 μs (step I). The $\delta(C_\beta C_c C_d)$ band intensity changed in 0.8−9 μs (step II), while the γ_7, ν_8, and $\delta(C_\beta C_c C_d)$ modes changed after >1 ms (step III). The temporal behavior of the spectral changes in step I was found to be ligand-dependent. Different temporal behavior was observed for *Sm*FixL and *Sm*FixLH2, suggesting that the observed structural changes of the heme and the heme pocket are linked to changes in the kinase domain. Structural changes occurring upon ligand dissociation, proposed on the basis of these time-resolved RR spectra, are schematically summarized in Figure 9. On the basis of the observed spectral changes, we propose the following hypotheses to explain the structural changes in FixL following ligand dissociation, and the mechanism of signal transduction.

Step I. Upon O_2 dissociation, intensity changes were observed for the ν(Fe−His), γ_7, and ν_8 bands after 0.3 and 1−2 μs for *Sm*FixLH2 and *Sm*FixL, respectively, in the earliest phase. Such changes in 10^{-7}−10^{-6} s region were not evident in the spectral changes occurring upon CO dissociation. Therefore, the structural change occurring in step I is relevant to discrimination of a ligand by FixL.

The intensity of the ν_8 band changed upon O_2 dissociation, but not upon CO dissociation in the region of 10^{-7}−10^{-6} s. It has been suggested that the intensity of this band is correlated with disorder in the orientation of the propionate groups (*21*). As the level of this disorder increases, the ν_8 band intensity decreases. For example, the ν_8 band of hemoglobin appeared when the heme propionates were motionally restricted in a trehalose glass (*22*). Arg214 has been proposed to play an important role in signal transduction by FixL. X-ray crystallographic data suggest that heme propionate 7 forms a salt bridge to Arg214 upon formation of the deoxy form from the oxy form. However, interactions between heme propionate 7 and its surroundings would not change significantly upon formation of the deoxy form from the CO-bound form because, in both structures, Arg214 forms a salt bridge to heme propionate 7. The fact that the intensity change of the ν_8 band in 10^{-7}−10^{-6} s was observed only upon O_2 dissociation suggests that the intensity change is associated with a structural change specific to O_2 dissociation. Accordingly, the increase in ν_8 band intensity is attributed to the formation of a salt bridge between Arg214 and heme propionate 7, which restricts the orientation of heme propionate 7.

The γ_7 mode is associated with an out-of-plane motion of the methine carbons. This band is observed in the high-spin complexes (met and deoxy forms) of myoglobin, but not in the low-spin adducts (the CO-bound and cyanomet forms) (*20*). This pattern is consistent with the out-of-plane intensity depending on an out-of-plane distortion of the heme group, since the Fe atoms are out of the heme plane in the high-spin complexes but in the plane in the low-spin complexes. Therefore, the intensity change of the γ_7 band is indicative of the extent of heme doming. On the basis of RR spectroscopic (*23*) and X-ray crystallographic (*8*) studies, it has been proposed that removal of Arg220 in *Bj*FixL results in flattening of the heme in FixL in both its ferric and ferrous states. Therefore, it is highly likely that the formation of the salt bridge between Arg214 and heme propionate 7 intensifies heme doming and thus intensifies the γ_7 band. In RR spectra of the heme, the band due to the γ_6 mode, another A_{2u} mode, is observed at 320−340 cm^{-1}. Although the γ_6 band has a low intensity in the FixL spectra, some portion of the intensity increase of the 345 cm^{-1} band may be due to the intensity increase of the γ_6 band. If it is the case, the increase of the γ_6 band intensity also suggests the intensified heme doming.

The ν(Fe−His) mode is one of the most intense Raman bands in myoglobin and hemoglobin because the heme is covalently linked to the protein solely through the proximal His; consequently, this mode is a good indicator of heme protein tertiary and quaternary structure (*24*). Bangcharouenpaurpong et al. (*25*) have proposed the origin of the intensity of the ν(Fe−His) mode results from orbital overlap between the σ* orbital of the Fe−His bond ($\sigma^*_{Fe-N_{His}}$) and the π* orbital of the porphyrin ring (π^*_{por}), which is small in the planar structure but becomes large in the domed structure.

An increase in ν(Fe−His) intensity was observed for *Sm*FixL and *Sm*FixLH2 upon O_2 dissociation. The intensity change of the γ_7 band suggests that formation of the salt bridge between Arg214 and heme propionate 7 results in greater heme doming. This increase can therefore be attributed to the increase in the extent of heme doming upon formation of the salt bridge in the O_2-dissociated species. On the basis of X-ray crystallographic data, Arg200 in the F helix forms a hydrogen bond to heme propionate 6 in the oxy form, whereas the hydrogen bond is cleaved in the deoxy form because Arg214 forms a salt bridge with heme propionate 7. These results suggest another possibility to account for the intensity change of the ν(Fe−His) band. Upon O_2 dissociation, the hydrogen bond between heme propionate 6 and Arg200 is cleaved, inducing a structural change in the F helix and, therefore, a change in the proximal histidine,

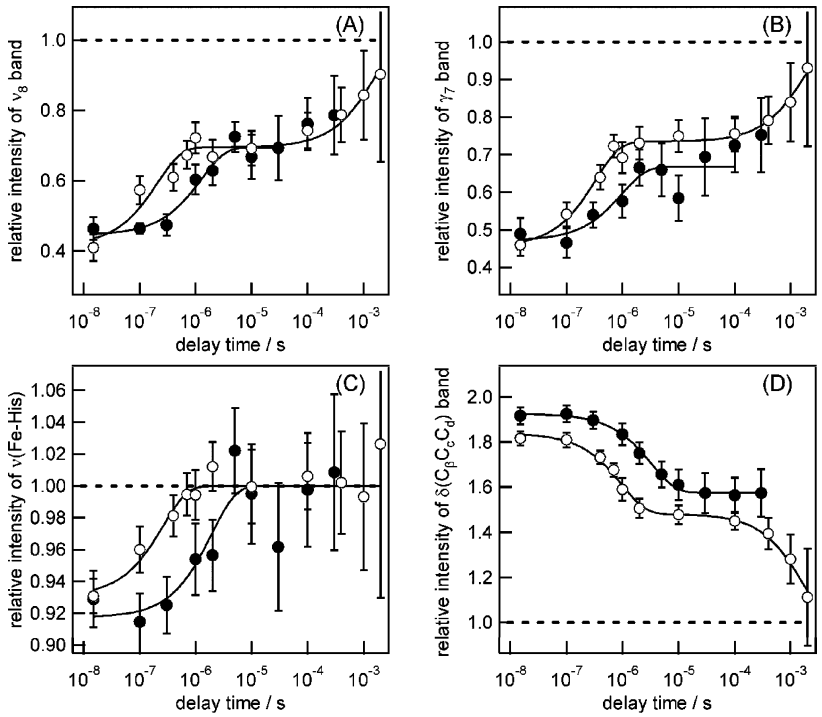

FIGURE 7: Logarithmic time plots of relative intensities for the γ_7, ν_8, ν(Fe−His), and $\delta(C_\beta C_c C_d)$ bands extracted from time-resolved data following O_2 dissociation. The filled and empty circles represent the relative intensities of *Sm*FixL and *Sm*FixLH2, respectively. The solid lines indicate the best fit obtained using an exponential decay or a sum of two exponential decays.

Table 1: Time Constants of Temporal Evolution of Raman Intensities of FixL[a]

	O_2 dissociation			CO dissociation	
	τ_1 (μs)	τ_2 (μs)	τ_3 (ms)	τ_2 (μs)	τ_3 (ms)
*Sm*FixLH2					
ν(Fe−His)	0.26 ± 0.17				
	(−0.69 ± 0.02)				
γ_7	0.33 ± 0.12		1.7 ± 0.4		0.20 ± 0.18
	(−0.28 ± 0.03)		(−0.27 ± 0.02)		(−0.13 ± 0.05)
ν_8	0.21 ± 0.16		1.5 ± 0.7		0.32 ± 0.30
	(−0.28 ± 0.08)		(−0.30 ± 0.03)		(−0.24 ± 0.04)
$\delta(C_\beta C_c C_d)$		0.96 ± 0.27	1.6 ± 0.3	0.77 ± 0.49	1.4 ± 1.0
		(0.36 ± 0.04)	(0.49 ± 0.03)	(0.36 ± 0.08)	(0.50 ± 0.02)
*Sm*FixL					
ν(Fe−His)	1.8 ± 1.5				
	(0.83 ± 0.02)				
γ_7	1.1 ± 0.9		nd[b]		nd[b]
	(−0.20 ± 0.07)		(−0.29 ± 0.07)		(−0.33 ± 0.03)
ν_8	1.3 ± 0.6		nd[b]		nd[b]
	(−0.25 ± 0.04)		(−0.33 ± 0.04)		(−0.30 ± 0.03)
$\delta(C_\beta C_c C_d)$		3.3 ± 0.5	nd[b]	9.1 ± 3.9	nd[b]
		(0.34 ± 0.02)	(0.58 ± 0.01)	(0.33 ± 0.05)	(0.61 ± 0.05)

[a] The temporal evolution is fitted to an exponential decay or a sum of exponential decays. The numbers in parentheses are the amplitudes of the exponential decays. The uncertainties are 90% confidence levels in the curve fitting. [b] Not determined due to instrument limitations for the time delay.

His194. Thus, the observed intensity change can be reasonably explained on the basis of the change in the Fe−His linkage and/or the change in heme doming.

The following proposed structural changes occur in step I (see Figure 9). In the O_2-bound form, Arg214 is hydrogen bonded to the bound O_2. Upon O_2 dissociation, Arg214 reorients toward heme propionate 7 and forms a salt bridge to it. The formation of this salt bridge restricts the orientation of heme propionate 7 and intensifies heme doming. These structural changes were observed as intensity changes of the ν_8, γ_7, and ν(Fe−His) bands in the time-resolved RR spectra. The formation of this salt bridge also gives rise to the dissociation of Arg200 and the heme propionate, which causes rearrangement of helix F, perturbing the Fe−His194 (the proximal histidine) linkage and inducing the intensity change of the ν(Fe−His) band. The intensities of the ν_8, γ_7, and ν(Fe−His) bands consistently changed in approximately 300 ns for *Sm*FixLH2 and 1−2 μs for *Sm*FixL. Thus, these data suggest that Arg214 is repositioned with these time constants in step I. The hydrogen bond between the bound O_2 and Arg214 has been discussed in a recent study of ultrafast absorption spectroscopy on the heme domain *Bj*FixL, which has revealed that the Soret band in the transient spectra after the photodissociation was blue-shifted compared to that of the deoxy form. Among three ligands (CO, NO, and O_2), the shift was largest for O_2. The largest

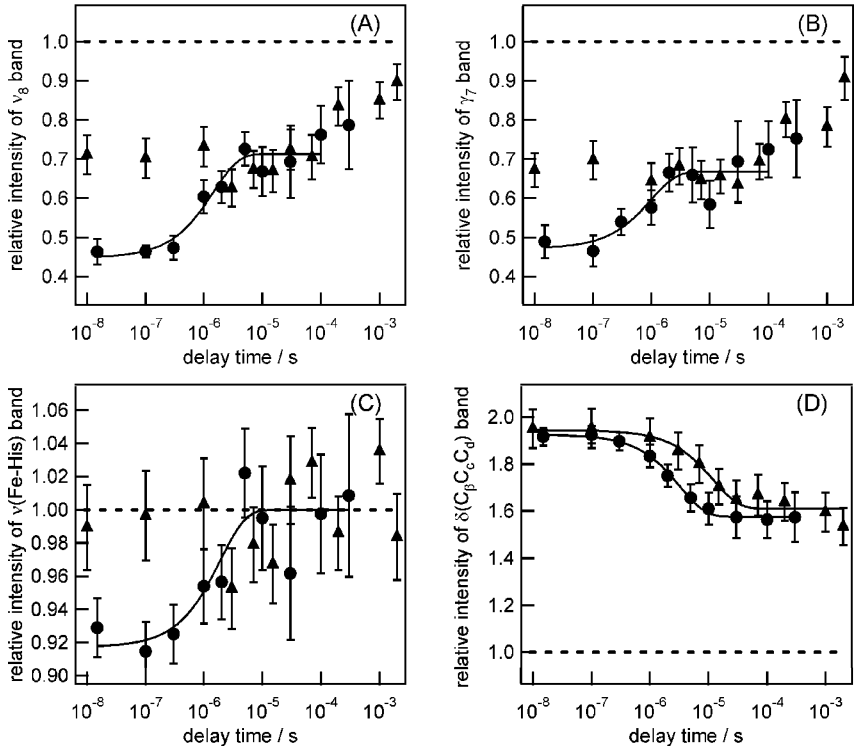

FIGURE 8: Logarithmic time plots of relative intensities for the γ_7, ν_8, ν(Fe−His), and $\delta(C_\beta C_c C_d)$ bands extracted from time-resolved data of *Sm*FixL. The filled triangles and circles represent the relative intensities of RR bands following CO and O_2 dissociation, respectively. The solid lines indicate the best fit obtained using an exponential decay or a sum of two exponential decays.

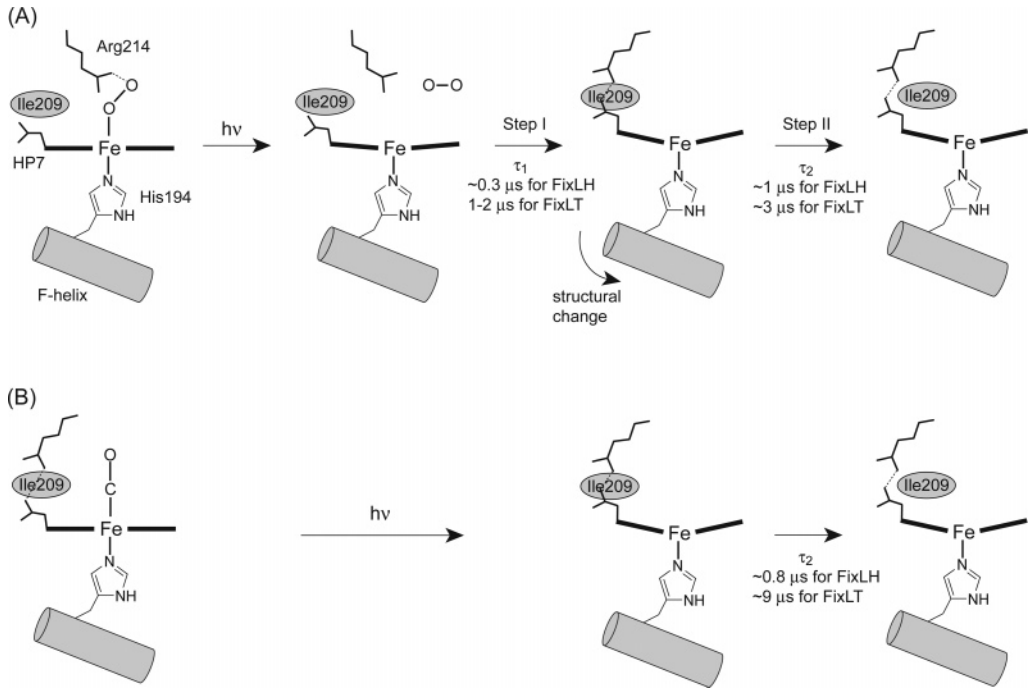

FIGURE 9: Scheme for structural changes occurring in the heme and in the vicinity of the heme in FixL following ligand dissociation. Support for this scheme is provided by the time-resolved RR spectra obtained in this study. HP7 denotes heme propionate 7.

perturbation relative to the deoxy spectrum was attributed to the presence of the hydrogen bond between the bound O_2 and Arg220 of *Bj*FixL.

Arg214 is a conserved residue among all known FixL proteins, and its equivalent is found in the distal pocket of the *Ec*DOS sensor protein (Arg97) (*26*). The X-ray structures of the sensor domain of FixL, as well as of *Ec*DOS, point to the importance of this residue, which interacts with the bound O_2 ligand. The spectral changes in step I are specific to the O_2-dissociated species, indicating that this is an important step for discrimination of the ligand by FixL.

Step II. Upon ligand dissociation, spectral changes were observed for the propionate $\delta(C_\beta C_c C_d)$ bending band in the 1−10 μs time range. The modes of the propionate are sensitive probes for the orientation and position of the porphyrin in the heme pocket, and of its interactions with the surrounding residues (*22*, *27*). The same intensity change was observed for both CO and O_2 dissociation, although the

rate of change was different, indicating that this intensity change is due to structural changes common to both the CO- and O_2-dissociated forms. Similar spectral changes were observed when Ile209 or Ile210 was replaced (*28*). Mukai et al. studied the roles of Ile209 and Ile210 in heme pocket structure and the regulation of histidine kinase activity by *Sm*FixL. RR spectra showed that the relative intensity of the $\delta(C_\beta C_c C_d)$ bands was different between WT and the mutants (I209W and I210H). Therefore, the change in the relative intensity of the $\delta(C_\beta C_c C_d)$ bands is consistent with the movement of Ile209 and Ile210.

These two isoleucine residues are strongly conserved in FixLs. The backbone amide of Ile209 is hydrogen bonded to heme propionate 6 in the ligand-bound forms, but this hydrogen bond is cleaved in the deoxy form. X-ray crystallographic data show different features in the electron density map of the deoxy and CO-bound forms, indicating structural differences in the FG loop centered on residue Ile206 and extending along the backbone of the FG loop to the adjacent residues, Ile209 and Gly211 (*29*). A prominent difference in electron density was visible on the heme propionate 6 side chain, which is hydrogen bonded to the backbone amide of Ile210. The side chain of Ile209 orients to the binding pocket in the deoxy form but cannot do so in the CO-bound form because of steric hindrance between the Ile209 side chain and the bound CO. Displacement of residues Ile209, Ile210, and Gly211 in the FG loop is also evident, accompanied by movement of heme propionate 6 with a change in iron ligation. Similar displacement was also reported for oxy-FixL (*10*). Thus, the repositioning of Ile209 and Ile210 is common to both the CO- and O_2-dissociated forms.

A similar spectral change was observed for the deoxy forms of R220 mutants (*23*, *30*) of the sensor domain, caused by the absence of a salt bridge between Arg214 and heme propionate 7. Therefore, changes in salt bridge strength may affect the relative intensity of the $\delta(C_\beta C_c C_d)$ bands. Structural rearrangement of the heme pocket on the microsecond time scale may cause a change in the strength of the salt bridge between Arg214 and heme propionate 7, so the possibility of structural changes in heme propionate 7 cannot be ruled out in step II.

To accommodate Ile209 in the heme pocket, either Arg214 or the dissociated CO must move away from the heme pocket in a manner consistent with the FG loop shift. In the case of the oxy form, Arg214 occupies the distal side of the heme pocket and must swing away from the heme pocket prior to changes in orientation of Ile209 and -210 in the O_2-dissociated form. In contrast, Arg214 is out of the heme pocket in the CO-bound form, so the orientation of Ile209 and -210 cannot change until the dissociated CO escapes from the heme pocket. Miksovska et al. (*31*) found that the dissociated CO leaves the heme pocket with a time constant of 150 ns. Therefore, the difference in the rate of change of the $\delta(C_\beta C_c C_d)$ bands can be due to differences in the rate-determining step between CO and O_2 dissociation.

Step III. For both CO and O_2 dissociation, changes to the spectrum of the deoxy form were not complete even after 2 ms; for some bands, the intensity showed the change in the millisecond time domain. Although we could not pursue structural changes in the deoxy structure due to instrument time delay limitations, at least one phase must occur on the millisecond time scale. In step III, the γ_7, ν_8, and $\delta(C_\beta C_c C_d)$ bands underwent changes in their intensities. Therefore, it is likely that the extent of heme doming, and interactions between the amino acid residues in the FG loop and the heme propionates, change during this phase. However, no intensity change was observed for the ν(Fe−His) band, indicating that there is no structural change in helix F in step III.

FG Loop Switch. These results imply that the interactions of the heme propionates with the distal residues, including Ile209, Ile210, and Arg214, change following O_2 dissociation. Residues Ile209, Ile210, and Arg214 are located in the FG loop region; therefore, movement of Arg214 and Ile209 or Ile210 must accompany the conformational change of the FG loop. The FG loop switch has been proposed as the structural change responsible for the catalytic control of the kinase domain in response to ligand binding at the sensor domain (*9*). This study suggests that downregulation of FixL is achieved by rearrangement of the FG loop by stepwise changes in Arg214 and Ile209 or Ile210 and that these changes are transmitted to the kinase domain for activation and/or inactivation of the catalytic site by intersubunit transduction (*32*). Arg214 is not repositioned in the CO-dissociated form, which could be why the spectral changes observed for the ν(Fe−His), γ_7, and ν_8 bands of the O_2-dissociated form in step I (10^{-7}−10^{-6} s) are missing, while the microsecond and submillisecond phases are present for those of the CO-dissociated form. In this view, the CO-bound state represents an intermediate in the mechanism, poised at the point where Arg214 is able to select against the heme-bound ligand. This could be the reason for the partial downregulation of the CO-bound form.

Comparison of Kinetics in SmFixLH2 and SmFixL. We have observed three steps in the time-resolved RR spectra of FixL upon ligand dissociation. These steps were lower in *Sm*FixL than in *Sm*FixLH2, suggesting that these structural changes are linked to the motion of the kinase domain and that the structural changes are relevant to signal transduction by FixL. This difference suggests coupling between the motion of the heme pocket and the kinase domain.

In step II, the diffusion of the dissociated ligand may be the rate-limiting step, raising another possibility to account for the difference in the rates of the intensity change of the $\delta(C_\beta C_c C_d)$ bands in *Sm*FixLH2 and *Sm*FixL. The rate of escape of CO from the heme pocket was reported to be accelerated by the elimination of 11 residues on the N-terminal end and 14 amino acid residues on the C-terminal end of the full-length sensor domain (*31*). Therefore, the difference in spectral rate change can be due to differences in the ligand escape rate in *Sm*FixL and *Sm*FixLH2. This suggests that the kinase domain affects the environment of the heme pocket. At present, we cannot judge which idea is more valid for explaining the difference between *Sm*FixLH2 and *Sm*FixL, but in either case, the results suggest that the kinase domain affects the heme pocket of the sensor domain.

CONCLUSIONS

We have examined structural changes in FixL from *Sinorhizobium meliloti* in investigating the mechanism of kinase inhibition by O_2. Time-resolved RR spectra for dissociation of the ligand from FixL spanning the picosecond to millisecond time regime showed that three steps in the structural changes occur following ligand dissociation.

Ligand-dependent structural changes were observed in step I. These results strongly suggest that Arg214 switches its interaction partner from the ligand O_2 to propionate 7 in ~300 ns and 1−2 μs for *Sm*FixLH2 and *Sm*FixL, respectively. Spectral changes in the time-resolved RR spectra are supportive of the FG loop displacement mechanism, with similar spectral changes being observed for both *Sm*FixL and *Sm*FixLH2. However, the rate of change was smaller for the former than for the latter, suggesting that the structural changes in the heme pocket are coupled to those in the kinase domain.

ACKNOWLEDGMENT

We thank Drs. Kazuhisa Yamamoto and Yasuo Kitaoka of Matsushita Electric Industrial Co., Ltd., for allowing us to use their frequency-doubled diode laser.

SUPPORTING INFORMATION AVAILABLE

Time-resolved RR spectra at the indicated delay times following the photolysis of CO- and oxy-*Sm*FixLH2. This material is available free of charge via the Internet at http://pubs.acs.org.

REFERENCES

1. Stock, J. B., Ninfa, A. J., and Stock, A. M. (1989) Protein phosphorylation and regulation of adaptive responses in bacteria, *Microbiol. Rev. 53*, 450−490.
2. Gilles-Gonzalez, M. A., Ditta, G. S., and Helinski, D. R. (1991) A haemoprotein with kinase activity encoded by the oxygen sensor of *Rhizobium meliloti*, *Nature 350*, 170−172.
3. Fisher, R. F., and Long, S. R. (1992) *Rhizobium*-plant signal exchange, *Nature 357*, 655−660.
4. Stock, A. M., Robinson, V. L., and Goudreau, P. N. (2000) Two-component signal transduction, *Annu. Rev. Biochem. 69*, 183−215.
5. Taylor, B. L., and Zhulin, I. B. (1999) PAS domains: Internal sensors of oxygen, redox potential, and light, *Microbiol. Mol. Biol. Rev. 63*, 479−506.
6. Gong, W., Hao, B., Mansy, S. S., Gonzalez, G., Gilles-Gonzalez, M. A., and Chan, M. K. (1998) Structure of a biological oxygen sensor: A new mechanism for heme-driven signal transduction, *Proc. Natl. Acad. Sci. U.S.A. 95*, 15177−15182.
7. Tuckerman, J. R., Gonzalez, G., Dioum, E. M., and Gilles-Gonzalez, M. A. (2002) Ligand and oxidation-state specific regulation of the heme-based oxygen sensor FixL from *Sinorhizobium meliloti*, *Biochemistry 41*, 6170−6177.
8. Dunham, C. M., Dioum, E. M., Tuckerman, J. R., Gonzalez, G., Scott, W. G., and Gilles-Gonzalez, M. A. (2003) A distal arginine in oxygen-sensing heme-PAS domains is essential to ligand binding, signal transduction, and structure, *Biochemistry 42*, 7701−7708.
9. Gong, W., Hao, B., and Chan, M. K. (2000) New mechanistic insights from structural studies of the oxygen-sensing domain of *Bradyrhizobium japonicum* FixL, *Biochemistry 39*, 3955−3962.
10. Hao, B., Isaza, C., Arndt, J., Soltis, M., and Chan, M. K. (2002) Structure-based mechanism of O_2 sensing and ligand discrimination by the FixL heme domain of *Bradyrhizobium japonicum*, *Biochemistry 41*, 12952−12958.
11. Miyatake, H., Mukai, M., Park, S. Y., Adachi, S., Tamura, K., Nakamura, H., Nakamura, K., Tsuchiya, T., Iizuka, T., and Shiro, Y. (2000) Sensory mechanism of oxygen sensor FixL from *Rhizobium meliloti*: Crystallographic, mutagenesis and resonance Raman spectroscopic studies, *J. Mol. Biol. 301*, 415−431.
12. Jain, R., and Chan, M. K. (2003) Mechanisms of ligand discrimination by heme proteins, *J. Biol. Inorg. Chem. 8*, 1−11.
13. Perutz, M. F., Paoli, M., and Lesk, A. M. (1999) Fix L, a haemoglobin that acts as an oxygen sensor: Signalling mechanism and structural basis of its homology with PAS domains, *Chem. Biol. 6*, R291−R297.
14. Mizutani, Y., and Kitagawa, T. (1997) Direct observation of cooling of heme upon photodissociation of carbonmonoxy myoglobin, *Science 278*, 443−446.
15. Mizutani, Y., and Kitagawa, T. (2001) Ultrafast Structural Relaxation of Myoglobin Following Photodissociation of Carbon Monoxide Probed by Time-Resolved Resonance Raman Spectroscopy, *J. Phys. Chem. B 105*, 10992−10999.
16. Rodgers, K. R., Lukat-Rodgers, G. S., and Tang, L. (1999) Spectroscopic Observation of a FixL Switching Intermediate, *J. Am. Chem. Soc. 121*, 11241−11242.
17. Tanaka, A., Nakamura, H., Shiro, Y., and Fujii, H. (2006) Roles of the heme distal residues of FixL in O_2 sensing: A single convergent structure of the heme moiety is relevant to the downregulation of kinase activity, *Biochemistry 45*, 2515−2523.
18. Franzen, S., Bohn, B., Poyart, C., and Martin, J. L. (1995) Evidence for sub-picosecond heme doming in hemoglobin and myoglobin: A time-resolved resonance Raman comparison of carbonmonoxy and deoxy species, *Biochemistry 34*, 1224−1237.
19. Kitagawa, T., Nagai, K., and Tsubaki, M. (1979) Assignment of the Fe-N_ϵ (His F8) stretching band in the resonance Raman spectra of deoxy myoglobin, *FEBS Lett. 104*, 376−378.
20. Hu, S., Smith, K. M., and Spiro, T. G. (1996) Assignment of Protoheme Resonance Raman Spectrum by Heme Labeling in Myoglobin, *J. Am. Chem. Soc. 118*, 12638−12646.
21. Peterson, E. S., Friedman, J. M., Chien, E. Y., and Sligar, S. G. (1998) Functional implications of the proximal hydrogen-bonding network in myoglobin: A resonance Raman and kinetic study of Leu89, Ser92, His97, and F-helix swap mutants, *Biochemistry 37*, 12301−12319.
22. Gottfried, D. S., Peterson, E. S., Sheikh, A. G., Wang, J., Yang, M., and Friedman, J. M. (1996) Evidence for Damped Hemoglobin Dynamics in a Room Temperature Trehalose Glass, *J. Phys. Chem. 100*, 12034−12042.
23. Balland, V., Bouzhir-Sima, L., Anxolabehere-Mallart, E., Boussac, A., Vos, M. H., Liebl, U., and Mattioli, T. A. (2006) Functional implications of the propionate 7-arginine 220 interaction in the FixLH oxygen sensor from *Bradyrhizobium japonicum*, *Biochemistry 45*, 2072−2084.
24. Kitagawa, T. (1987) The Heme Protein Structure and the Iron Histidine Stretching Mode, in *Biological Applications of Raman Spectroscopy* (Spiro, T. G., Ed.) pp 97−131, John Wiley & Sons, New York.
25. Bangcharoenpaurpong, O., Schomacker, K. T., and Champion, P. M. (1984) Resonance Raman investigation of myoglobin and hemoglobin, *J. Am. Chem. Soc. 106*, 5688−5698.
26. Park, H., Suquet, C., Satterlee, J. D., and Kang, C. (2004) Insights into signal transduction involving PAS domain oxygen-sensing heme proteins from the X-ray crystal structure of *Escherichia coli* Dos heme domain (Ec DosH), *Biochemistry 43*, 2738−2746.
27. Marzocchi, M. P., and Smulevich, G. (2003) Relationship between heme vinyl conformation and the protein matrix in peroxidases *J. Raman Spectrosc. 34*, 725−843.
28. Mukai, M., Nakamura, K., Nakamura, H., Iizuka, T., and Shiro, Y. (2000) Roles of Ile209 and Ile210 on the heme pocket structure and regulation of histidine kinase activity of oxygen sensor FixL from *Rhizobium meliloti*, *Biochemistry 39*, 13810−13816.
29. Key, J., and Moffat, K. (2005) Crystal structures of deoxy and CO-bound bjFixLH reveal details of ligand recognition and signaling, *Biochemistry 44*, 4627−4635.
30. Balland, V., Bouzhir-Sima, L., Kiger, L., Marden, M. C., Vos, M. H., Liebl, U., and Mattioli, T. A. (2005) Role of arginine 220 in the oxygen sensor FixL from *Bradyrhizobium japonicum*, *J. Biol. Chem. 280*, 15279−15288.
31. Miksovska, J., Suquet, C., Satterlee, J. D., and Larsen, R. W. (2005) Characterization of conformational changes coupled to ligand photodissociation from the heme binding domain of FixL, *Biochemistry 44*, 10028−10036.
32. Nakamura, H., Kumita, H., Imai, K., Iizuka, T., and Shiro, Y. (2004) ADP reduces the oxygen-binding affinity of a sensory histidine kinase, FixL: The possibility of an enhanced reciprocating kinase reaction, *Proc. Natl. Acad. Sci. U.S.A. 101*, 2742−2746.

BI062083N